Oral presentation | Industrial applications
Industrial applications-II
Tue. Jul 16, 2024 10:45 AM - 12:45 PM Room B

[4-B-01] Characterization of LES Inlet Conditions with Mapped Wingtip Vortices using UVLM Mean Flow Field Data

*Jia Cheng Chan[1], Peng Cheng Wang[2], James Jun Yuan Tan[3], Henrik Hesse[1], （1. University of Glasgow, 2. Singapore Institute of Technology, 3. ST Engineering Aerospace Ltd）

Keywords: Inlet conditions, Large Eddy Simulation, Unsteady Vortex Lattice Method, Synthetic inlet, Wake vortex surfing

Twelfth International Conference on Computational Fluid Dynamics (ICCFD12), Kobe, Japan, July 14-19, 2024

ICCFD12-2024- 0103

Characterization of LES Inlet Conditions with Mapped Wingtip Vortices using UVLM Mean Flow Field Data

J. C. Chan*, P. C. Wang**, J. J. Y. Tan*** and H. Hesse*

Corresponding author: j.chan.2@research.gla.ac.uk

* University of Glasgow, United Kingdom.

** Singapore Institute of Technology, Singapore.

*** ST Engineering Aerospace Ltd, Singapore.

Abstract: The circulation and roll-up of the wake panels in UVLM are used to derive the velocity components and characterize wingtip vortices for effective mapping onto the LES inlet boundary conditions. Validation of the simulation results with the mapped inlet discovering that the missing velocity fluctuations cause discrepancies in the vortex core behavior. Hence, incorporating a representative fluctuation profile from generated by LES is necessary to synthesize a realistic and accurate vortex flow and development.

Keywords: Inlet Conditions, Large Eddy Simulation, Unsteady Vortex Lattice Method, Synthetic Inlet, Wake Vortex Surfing.

1 Introduction

Wake vortex surfing [1, 2] inspired by migratory birds [3, 4] allows the trailing aircraft to benefit from surfing the updraft of the wingtip vortices generated by a leading aircraft. This results in higher lift, lesser induced drag [5] and reduced fuel consumption. Accurate prediction of wingtip vortices is critical to identifying the optimal formation spacing [6, 7] in longitudinal, lateral, and vertical direction. This concept can lead to reductions of greenhouse gas emissions without making modifications to the existing aircraft designs.

The concept of wake vortex surfing has been experimentally validated and showcased in military fighter jet [8, 9] and transport aircraft [10] within close-range formation flight and eventually expanded to commercial passenger aircraft [11, 12] in extended longitudinal range (up to $x/b = 57$). For such considerably large spacing between the aircraft in formation, the wingtip wake vortices from lead aircraft have developed into the mid to far field [13], making the behavior of the vortices more unpredictable. As wind tunnel experiments [14] are limited by the physical length of the test sections, computational fluid dynamics (CFD) simulation plays a crucial role in predicting the development of wingtip vortices further downstream, with the aim of identifying the beneficial region for trailing aircraft to surf on.

Some CFD simulations using Reynolds-Averaged Navier Stokes (RANS) [15, 16] models were conducted to analyze the optimal lateral and vertical position of unmanned aerial vehicle (UAV) in close formation ($x/b < 3$). The simulation outcomes were deemed largely positive, showing only minor deviations from the flight test results. However, the predictive accuracy of RANS model deteriorates going downstream of the field due to the limitation in persisting the wingtip vortices [17, 18]. Therefore, higher fidelity models such as Large Eddy Simulation (LES) [19, 20] or even Direct Numerical Simulation (DNS) [21] are necessary for accurately representing the flow field in extended formation flight. Vechtel et al. [22] utilized LES to simulate vortex flow fields with slight perturbations along the vortex lines, creating a more realistic flow field that reflects actual flight conditions. The simulation covered extended formations up to 62 wingspans in longitudinal direction.

The conventional CFD approach for simulating formation flight typically involves placing both the leading and trailing aircraft within a single continuous computational domain. Given the substantial spacing between aircraft in the extended formation, these simulations require robust computational resources resulting in high set-up and running cost. Thus, to reduce the cost, an alternative approach is to create a plane with an appropriate wake vortex profile and map it as the inlet boundary condition for the simulation domain of the trailing aircraft. The wake vortex is initiated and developed in a separated inlet condition (IC) domain before transferring the vortical flow data onto the inlet boundary of the main simulation (MS) domain. In this approach the vortex flow in the MS appears to be continuous from the IC domain, thereby achieving results comparable to those of a conventional single domain simulation. This allows repetitive simulation of MS only, without the computational overhead of simulating the entire domain.

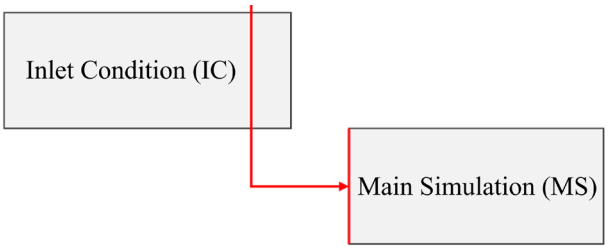

Figure 1: Inlet condition and main simulation

It is well known that the inlet condition is a complex yet critical part for the LES simulation [23]. Extensive research on the inlet condition have focused on regenerating the turbulent fluctuation at the inlet [24-33]. One of the simplest methods to reproduce the turbulent fluctuations involves introducing white noise, which gives a random variation in the fluctuations level, with consistent level of intensity at all frequencies. This method, however, has the significant drawback that it lacks in temporal and spatial coherence [24]. Any uncorrelated turbulent inlet conditions will greatly impact the flow field development and accuracy in the simulation domain downstream.

Hence, most research either focuses on precursor or synthetic methods. Tabor and Baba-Ahmadi [25, 26] have reviewed the various inlet boundary condition methods and highlighted the deficiency of basic mapping method in reproducing the accurate turbulence fluctuation. To address this limitation, Wang and McGuirk [23, 27, 28] have demonstrated the recycling-rescaling model (R^2M) by applying additional forcing mechanisms and explicit velocity correction into the system. Montorfano et al. [29] also reported that the internal plane mapping has the closest velocity profile to the theoretical law-of-the-wall as well as the fluctuation away from the wall. Villers [30] and Dhamankar and Blaisdell [31] used the pre-computed database approach, incorporating pre-existing periodic turbulence with rescaled phase-amplitude jittering to manipulate the CFD domain inlet boundary. Pierce and Moin [32] introduced an azimuthal body force to conquer the wall drag, and an axial body force to drive the physical flow for confined swirling inflow boundary conditions in LES. Jiang et al. [33] specified a swirling velocity profile with a desired swirl number, serving as the mean velocity profile for DNS and LES and adjustable by varying the body force. The proposed analytical solution agrees well with the simulation and experimental results for both annular and round jets. The literature above shows that the LES inlet conditions can be manipulated to produce the desired flow turbulence.

However, most existing work focus on near-wall turbulence in internal flows and confined simulation domains such as jet combustors. Few research addresses the inlet conditions involving wake vortex dynamics in freestream airflow. This gap exists for several reasons. Firstly, to model and store the time series data of inflow boundary conditions requires significant computational storage [34]. Moreover, the data cannot guarantee the turbulence quantities in the domain to be corresponding to prescribed target characteristics.

Although LES captures the vortex turbulent structures more accurately, the extension of wake vortex development into mid to far field [13] in the IC domain will exacerbate the computational cost of generating the wake dynamics, due to the need for fine spatial and temporal resolutions [35]. In this paper, the authors propose to employ the unsteady vortex lattice method (UVLM) [5, 36] as IC to provide the mean flow field data for LES MS. There are studies using similar models where mean velocity data generated from the upstream RANS [37] or vortex methods (VM) [38] are integrated with periodic LES velocity fluctuation profiles as inlet conditions for main simulation, but in the context of internal pipe flow.

The proposed hybrid method in this work utilizes the efficiency of UVLM to initialize the wake vortices as inlet conditions. At the same time, the simulation setup will be conducted with a validated LES framework [18] to generate the appropriate fluctuations profile which will be incorporated to synthesize and reproduce the turbulence on the mean velocity. This LES results also provides a validation database to the wake vortex modeled by UVLM.

2 Methodology

Due to the substantial longitudinal spacing in extended formation, the UVLM will be more efficient and cost effective in calculating the preliminary information on vortex roll-up and development around lifting surfaces. The UVLM is an extension of the Prandtl lifting line theory, where the aircraft main lifting surfaces are modelled as thin sheet vortex panels using Cartesian coordinates. The circulation of the trailing vortex in the UVLM is utilized to establish the baseline wake vortex information, including mean tangential and axial velocity, necessary for mapping as the inlet boundary conditions for the LES main simulation (MS).

The mean flow field from the UVLM is however not favorable for LES inlet boundary due to the lack of velocity fluctuations. In LES, the turbulent kinetic energy computation relies on the mean square fluctuations of velocity components, $\overline{u'u'}$ [39], which are derived from the resolved large-scale eddies. The accurate representation of the velocity fluctuations is also crucial for calculating the Reynolds stress tensor, $\tau_{ij} = \overline{u_i' u_j'}$, which plays a fundamental role in momentum transfer modeling and turbulent mixing process. As such, the velocity fluctuations components u' , v' and w' are deemed crucial parameters in LES [23]. These fluctuations play a significant role in reproducing the turbulent flow dynamics that facilitate the energy cascade from larger eddies to smaller ones, which is essential in momentum transport for predicting the wingtip vortices development in further downstream. Therefore, in this work the velocity fluctuations will be synthetically driven by a Fourier-transformed sinusoidal equation based on a representation of LES time series data.

With the LES precursor data, the velocity fluctuations are plotted in time domain and frequency domain by Fourier transform [40]. To match the IC velocity characteristics with the LES simulations, a synthetic forcing term is required to manipulate and rescale the inlet velocity. An LES simulation over the same leading wing will be conducted separately to generate the fluctuations profile of velocity components to the mean flow field data in IC.

2.1 Inlet Condition – Wingtip Vortex by UVLM

The lifting line theory [41] explains the mechanism of trailing vortices in the lift generation process. It conceptualizes a finite wing as having an infinite number of horseshoe vortices distributed along the aerodynamic centerline throughout the entire wingspan, as shown in Figure 2. The lifting line is created by the bound vortices that run across the aerodynamic centers of each airfoil segment of the wing.

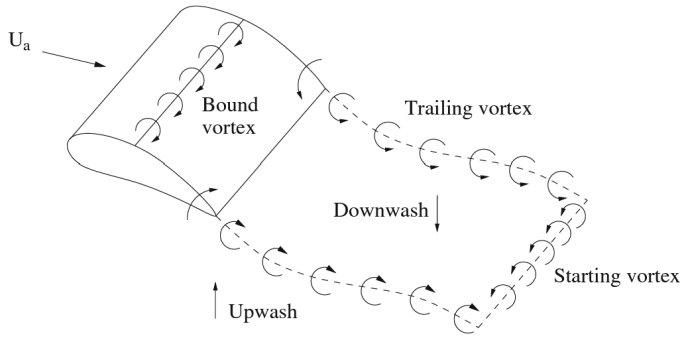

Figure 2: Horseshoe Vortex Model [41].

Building on the lifting line theory, the unsteady vortex lattice method (UVLM) [42, 36] uses a lattice of horseshoe vortices to discretize a lifting surface into multiple quadrilateral panels. UVLM treats the lifting area as a thin surface neglecting the influence of thickness. This method models fluid flow under incompressible, inviscid and irrotational conditions, commonly referred to as potential flow. In this framework, the velocity potential scalar φ satisfies the Laplace's equation, where $\nabla^2\varphi = 0$. The wake vortex lattices are transported from the trailing edge with vorticity of equivalent strength to the bound vortex lattices. The corner points of the free wake lattices move with the local velocity, and the following non-penetration condition is applied to all collocation points on the wings,

$$(u_b + u_w + u_\infty - u_k) \cdot n = 0 \tag{1}$$

where u_b denotes the induced velocity produced by bound vortex lattices, u_w denotes the induced velocity produced by wake vortex lattices, u_∞ denotes the freestream velocity, u_k denotes the surface kinematic velocity, and n denotes the local normal vector at the collocation point. Another boundary condition is that the flow disturbance diminishes at infinity, as follows,

$$\lim_{\|x-x_0\|\to\infty} u = 0 \tag{2}$$

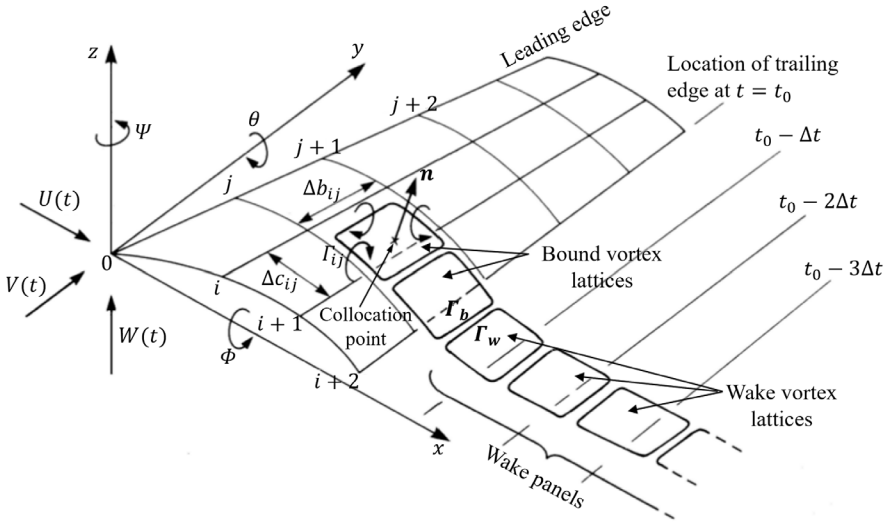

Figure 3: Descriptive diagram of UVLM [69].

The induced velocities at each point induced by the horseshoe vortices are calculated using the Biot-Savart law. In flight condition, the UVLM models the force-free wake by forming vortex rings over the mean panel surface, as shown in Figure 3. Each discretized quadrilateral panel is attached with bound

vortex lattices, where the leading vortex ring is placed on the panel's quarter-chord line and the rear vortex ring is placed on the next panel's quarter-chord line. The collocation point is on the three-quarter chord line, which falls at the center of the vortex ring.

The UVLM toolkit utilized in this study is SHARPy (Simulation of High-Aspect-Ratio aircraft and wind turbines in Python) [43, 44]. It is an open-source software package well-known for simulation of nonlinear aeroelastic systems, integrating structural dynamics and aerodynamic solvers [45, 46]. The UVLM is solving a system of linear algebraic equations to determine the singularity strengths at every time step [47, 48]. The induced velocity at an arbitrary field point, r due to a vortex lattice with vertices $P = \{P^i, i \in [1,4]\}$ and strength Γ can be expressed by $u(r) = A(P,r)\,\Gamma$, where $A(P,r)$ denotes the three-dimensional influence coefficient. At discrete time step $n+1$, the vorticity distribution of the bound vortex elements is determined by applying the non-penetration boundary condition, formulated as,

$$A_{cb}\Gamma_b^{n+1} + A_{cw}\Gamma_w^{n+1} + w^{n+1} = 0 \tag{3}$$

where A_{cb} and A_{cw} denotes bound-to-collocation and wake-to-collocation aerodynamic influence coefficient matrices, Γ_b and Γ_w are the circulation strength vector for bound and wake vortex rings, and $w = (u_\infty - u_k)\cdot n$ represents the normal component of all velocities except those induced by bound and wake vortex lattices at the collocation points. The induced velocity is calculated at the field points to obtain the influence matrices and the convection velocity of the wake, before the equation solves both the bound and wake vortex strength vector Γ_b and Γ_w iteratively.

The velocity induced by a vortex ring l over collocation point k can be calculated using the Biot–Savart law. For a unit circulation strength, it is expressed as,

$$\vec{u}_{i,kl} = \oint_{C_l} \frac{d\vec{s}_l \times \vec{r}_{kl}}{4\pi|\vec{r}_{kl}|^3} \tag{4}$$

where $d\vec{s}_l$ represents the differential element of the vortex segment along the ring l, that makes up the complete ring C_l, and $\vec{r}_{kl}$ is the vector from the collocation point k to the relevant vortex ring at l. This process involves four evaluations of the Biot-Savart law, corresponding to each vortex segment of the closed circuit C_l. The aerodynamic influence coefficient matrices A_{cb} and A_{cw} are determined by calculating all cross-induced velocities at the collocation points and projecting these velocities along the normal vector of the respective panel,

$$(A_{cb})_{kl} = \vec{u}_{i,kl}\vec{n}_k, \qquad k,l = 1 \dots N_b \tag{5}$$

$$(A_{cw})_{kv} = \vec{u}_{i,kv}\vec{n}_k, \qquad k,l = 1 \dots N_b, \qquad v = 1 \dots N_w \tag{6}$$

where k, l are bound (surface) panel counters, v is the vortex ring counter, and N_b is the number of total bound panels, N_w the number of wake panels, and n_k is the total number i the normal vector of the kth vortex ring (at which the induced velocity is being computed. The propagation equation for the wake circulation can be written in discrete time as follows,

$$\Gamma_w^{n+1} = C_{\Gamma b}\Gamma_b^n + C_{\Gamma w}\Gamma_w^n \tag{7}$$

where $C_{\Gamma b}$ and $C_{\Gamma w}$ map the circulation of the previous time step to the current one, and they are very sparse constant matrices which account for Kelvin's circulation theorem, which mandates that the total circulation of the vortex sheet shed from the trailing edge of the wing remains constant as it moves downstream. Additionally, these matrices also comply with Helmholtz's vortex theorem in the convection of the wake, which leads to the rolling up of the wake panels into the concentrated wingtip vortex structure.

Once the flow is fully developed, the roll-up of the wake panels downstream captures the formation of wingtip vortices, which is utilized to determine the vortex core center locations (y_c, z_c) and their respective core radius, r_c. This process helps to establish the initial shape and size of the vortex core. The circulation strength calculated from the UVLM is used then to provide data to define the tangential velocity field of the vortical flow by the Lamb-Oseen model [49, 50],

$$u_\theta = \frac{\Gamma_v}{2\pi r}\left[1 - e^{-1.26\left(\frac{r^2}{r_c{}^2}\right)}\right] \tag{8}$$

where the circulation of wingtip vortex, Γ_v is approximately equal to the spanwise-averaged circulation strength [51, 52]. A higher Γ_v typically indicates stronger vortices, or tangential velocity. The tangential velocity at any point (y, z) is calculated based on the radial distance, r, from the vortex core center,

$$r = \sqrt{(y - y_c)^2 + (z - z_c)^2} \tag{9}$$

The tangential velocity can then be decomposed into Cartesian velocity components u_y and u_z using trigonometeri relationships and is the angle θ from the selected point to the vortex core center,

$$u_y = -u_\theta \sin\theta \tag{10}$$

$$u_z = u_\theta \cos\theta \tag{11}$$

After establishing the tangential velocity, the only velocity component remaining for the inlet condition is the axial velocity u_x. As wingtip vortices develop, the surrounding airflow curls inward and revolves around the center of the vortex core. This dynamic mechanism creates an axial velocity excess right after the wing trailing edge, and subsequently transitions into a deficit after a certain distance [53, 54]. The axial velocity profile typically shows a deficit of 15% at the center of the core and it tends to restore to freestream velocity at about one to two core radius distance from the core center [55],

$$u_x = u_\infty \cdot \left[1 - 0.15\, e^{-1.26\left(\frac{r^2}{r_c{}^2}\right)}\right] \tag{12}$$

With the three-dimensional velocity components derived from the UVLM, inlet boundary conditions can be specified for the LES main simulation domain. While the inflow data does not fully capture the required dynamic complexities, it does provide initial vortex data to initiate the simulation with high efficiency. Validation on the vortices will be performed to assess the accuracy of this approach.

2.2 Main Simulation – Synthesized Velocity Fluctuations from LES

LES resolves the large eddies which contain most of the turbulent kinetic energy. The resolved turbulent kinetic energy and the Reynolds stress tensor rely heavily on the velocity fluctuation components. Hence, the mean flow field data from the UVLM is insufficient to map directly onto the LES inlet boundary. The lack of velocity fluctuation components causes the wake vortex to vanish rapidly in the near downstream [23] and cannot replicate the realistic wake vortex form. To overcome the issue, the velocity fluctuations u', v' and w' are often the important parameters in LES [23] to reproduce the turbulent fluctuations and the wingtip vortex development in the downstream over a long distance.

A prior simulation with identical set-up in LES has been conducted [18]. The spatially and temporally coherent turbulence from the LES will be utilized to synthesize the turbulence on the UVLM mean

velocity field. OpenFOAM (Open-source Field Operation and Manipulation) [56] is utilized as the CFD software in this research. It is extensively used in CFD application and has proven robustness in capturing wake and turbulences phenomena [57, 58]

The Smagorinsky model [59] is employed as the LES sub-grid scales (SGS) model in the current work due to its simplicity and effectiveness in handling a variety of turbulent flows. The governing equations of unsteady 3D incompressible flow with the subgrid scale stress tensor, τ_{ij}^{sgs} from Smagorinsky model for LES [39] is as follows,

$$\frac{\partial \rho \tilde{u}_i}{\partial t} + \rho \tilde{u}_j \frac{\partial \tilde{u}_i}{\partial x_j} = -\frac{\partial \tilde{p}}{\partial x_i} - \frac{\partial}{\partial x_j}\left(\tau_{ij} + \tau_{ij}^{sgs}\right) \tag{13}$$

The tilde accent indicates spatial filtering using a three-dimensional filter of size Δ. $\tilde{u}_i$ and $\tilde{p}$ denote the filtered velocity and pressure. The SGS stress tensor τ_{ij}^{sgs} represents the influence of unresolved turbulence, consisting of anisotropic and isotropic parts,

$$\tau_{ij}^{sgs} = a_{ij}^{sgs} + \frac{2}{3} k_r \delta_{ij} \tag{14}$$

The anisotropic part, a_{ij}^{sgs} is correlated with the Smagorinsky eddy viscosity, μ^{sgs}, the filtered strain rate tensor, $\tilde{S}_{ij}$, and the Smagorinsky constant, C_S which is taken as 0.18 here.

$$a_{ij}^{sgs} = -2\mu^{sgs}\tilde{S}_{ij} \tag{15}$$

$$\mu^{sgs} = \tilde{p}(C_S\Delta)^2\left|\tilde{S}_{ij}\right| \tag{16}$$

For the turbulent kinetic energy, k_r in the anisotropic part, it is defined as follows,

$$k_r = \frac{1}{2}\tau_{ij}^{sgs} \tag{17}$$

Finally, the subgrid scale stress tensor is formulated with the above constants and variables,

$$\tau_{ij}^{sgs} = 2\mu^{sgs}\tilde{S}_{ij} - \frac{2}{3}\rho k_r \delta_{ij} \tag{18}$$

LES exhibits relatively high fidelity due the fact that the isotropic part constitutes a minor portion of the total energy field [60]. By refining the mesh grid, the sub-grid scale volume is reduced, and accuracy of the model is enhanced further. The recommended mesh grid size is ranged from 3% to 10% of the characteristic dimension of geometry (wing chord length in this case), as stipulated by requirements [61]. However, based on the preceding validation study of the vortex core characteristics [18], the mesh cell size within the volume surrounding the vortex core is set to approximately 1.1% chord length. To ensure the maximum Courant number below one across the entire flow field, a time-step of 1×10^{-5}s is utilized.

The simulation is running for 50 chord-flow times to stabilize the transient effects and establish a statistically steady flow rate [62]. The velocity data in the time series is subsequently recorded for another 50 chord-flow times to ensure thorough and precise acquisition of velocity fluctuations pattern over an adequately prolonged duration. The LES fluctuations in time domain are later transformed into frequency domain by Fourier transform [40]. From the frequency domain plot, the fluctuations amplitude, frequency and phase lag can be identified and form a series of sinusoidal functions to reproduce the time-dependent velocity fluctuations, $u'_{i,j,k}(t)$ as follows,

$$u'_{i,j,k}(t) = \bar{u}_{i,j,k} \cdot \left[\sum_{\kappa=1}^{n} a_{i,j,k} \cos\left(\kappa_{i,j,k} t + \varphi_{i,j,k}\right) + \sum_{\kappa=1}^{n} b_{i.j.k} \sin\left(\kappa_{i,j,k} t + \varepsilon_{i,j,k}\right)\right] \quad (19)$$

where $\bar{u}_{i,j,k}$ is the time-averaged velocity at position (i, j, k) from the UVLM. The $a_{i,j,k}$ and $b_{i.j.k}$ are coefficients determining the amplitude of the cosine and sine components respectively, $\kappa_{i,j,k}$ are frequencies associated with each term, and $\varphi_{i,j,k}$ and $\varepsilon_{i,j,k}$ are phase lag. The summation of the trigonometric components introduces periodic fluctuations with specific frequencies and phase angle to generate synthetic fluctuations, in relation to its correlated mean velocity magnitude. Combined with the Fourier series turbulence data created based on the periodic LES data, the mean flow field solutions from the IC, using LES, RANS or even vortex method [63], can transform the desired velocity data to be applied on MS inlet boundary,

$$u_{i,j,k}(t) = \bar{u}_{i,j,k}^{UVLM} + u'^{LES}_{i,j,k}(t) \quad (20)$$

Turbulent inlet conditions with synthesized fluctuations from LES consume less computer memory as compared to precursor method [64], since the turbulence is regenerated at each time step of the LES computation and eliminating the need to store the extensive time series of velocity fluctuations. This method also maintains the continuity conditions during the inlet fluctuations generation process [65].

3 Results

This study compares the outcomes of UVLM against literature data to determine the appropriate plane for serving as the LES vortex inflow condition. The absence of temporal fluctuations in UVLM leads to some discrepancies in the vortex characteristics downstream of the inlet boundary. To address the issue, velocity fluctuations from a LES simulation are processed to derive an equation for reproducing the fluctuations synthetically. The detailed analysis of velocity fluctuations across the vortex core within the LES is conducted, aims to improve the accuracy and applicability of the synthetized method on the vortex inlet condition.

3.1 UVLM Data for LES Inlet Conditions

The wing model geometry and stream field conditions employed for this research are derived from the validated simulation presented in the literature [18]. The wing geometry is a symmetrical airfoil (NACA0012) profile with a chord length of $0.14m$, a semispan of $0.15m$, and an angle of attack, α of 10°. The freestream velocity is $34m/s$ in x-direction, not having dynamic inputs such as gusts and turbulence. This case set-up assumes a rigid-body condition, neglecting the aeroelastic effects such as wing deformation under aerodynamic loads.

In the UVLM, each wake panel induces velocities in the surrounding fluid and experiences velocities induced by all other panels, causing the wake to move and rotate. The positions of wake panels are iteratively updated based on these induced velocities, ensuring compliance with Kelvin's circulation theorem and Helmholtz's vortex theorems. These principles collectively caused the wake panels to roll up as they convect downstream, forming coherent and concentrated tip vortex structures. The force-free wake roll-up modelled by the UVLM is presented in Figure 4. This illustration shows the evolution of the wake behind the wing in a steady freestream flow field condition. It shows the wake circulation strength, Γ_p peaking at the mid-span and gradually decreasing towards the wingtip, in an elliptically distributed profile. As the wake progresses in the streamwise direction, it is observed that the roll-up phenomenon becomes more prominent, leading to a noticeable enlargement in the wingtip vortex structures.

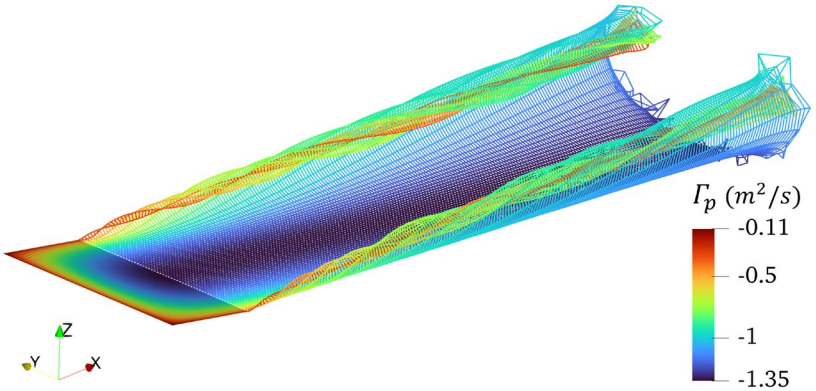

Figure 4: Force-free wake roll-up modelled by UVLM, colored by panel circulation Γ_p.

The wingtip vortex represented by the spanwise wake panel roll-up are captured at every chord length interval along the freestream direction, as shown in Figure 5. The wingtip vortex circulation, Γ_v can be approximated using the spanwise-averaged wake circulation, where $\Gamma_v \approx \bar{\Gamma}_w$ at the corresponding longitudinal position [52]. The spanwise-averaged circulation is also perceived as $\bar{\Gamma}_w = \pi\Gamma_0/4$, where Γ_0 is the maximum circulation strength at the midspan or wing root position ($y = 0$). To affirm the vortex circulation strength estimated by the UVLM, a validation is conducted against the reported values in LES, URANS and experimental studies [66]. As shown in Figure 6, the UVLM results fall within the reported range.

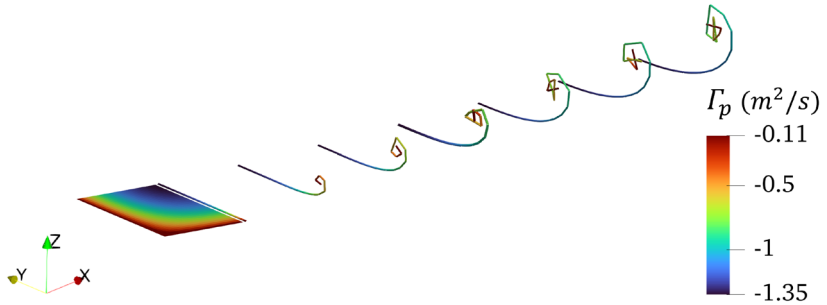

Figure 5: Development of wingtip vortex per chord distance downstream.

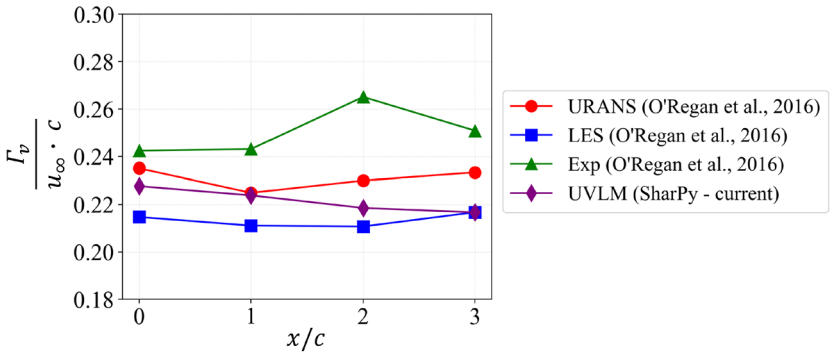

Figure 6: Validation of normalized vortex circulation strength with downstream distance.

At plane $x/c = 0$, the wake panel does not exhibit any roll-up behavior due to the vortex lattice at this position is still closely attached to the trailing edge bound panel. However, as the force-free wake panels roll up and progress downstream, they form into wingtip vortex structures which provide measurable data to determine the dimension and position of the vortex core. Figure 7 shows the downstream view on the vortex filament roll-up development, illustrating the presence of vortex core in relative to the wing panel (color plot in the background).

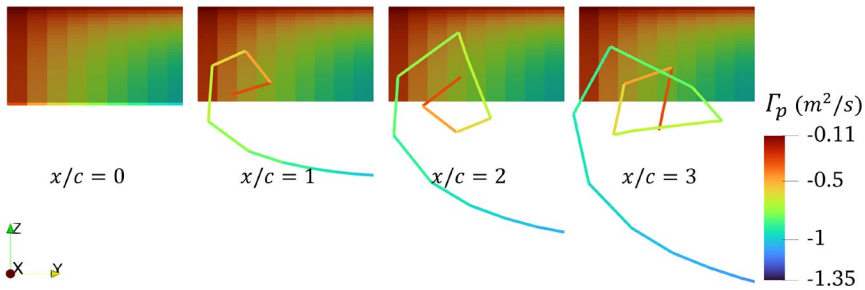

Figure 7: Wake panel roll-up in the vortex core region, view from downstream.

In this study, the authors identified that the vortex filaments with an overall roll-up angle exceeding 90° are within the vortex core region. This significant rotation indicates the presence of concentrated vortex structures typical of wingtip vortices. With the vortex core region identified, the vortex core center is computed by averaging the vertex coordinates of all vortex filament within that area. Subsequently, the radial distances from this center point to each filament vertex are averaged to determine the vortex core radius, r_c. The vortex core characteristics are then plotted alongside the refence data [18, 66] for comparison, as illustrated in Figure 8.

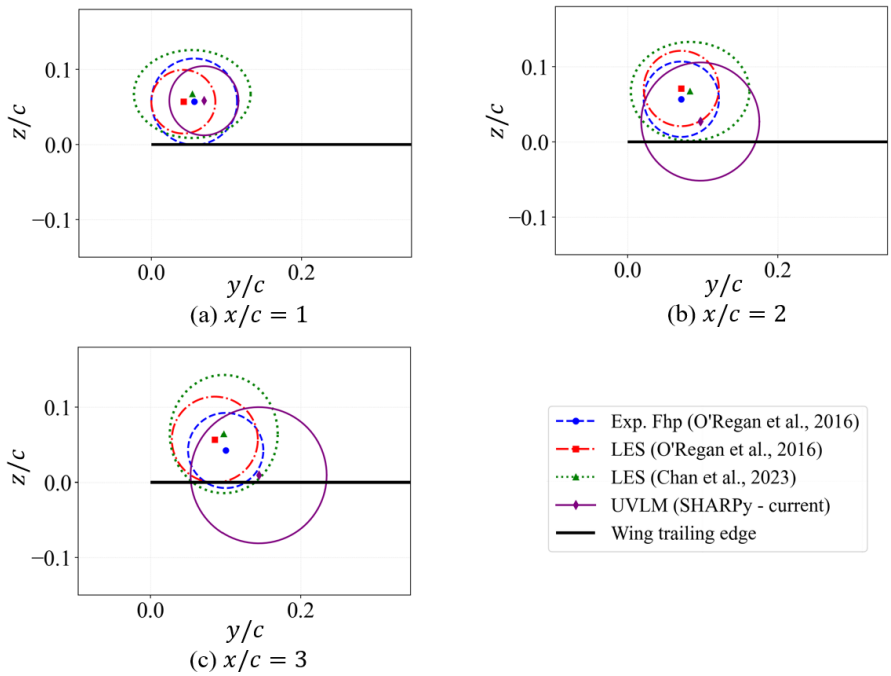

Figure 8: Comparison on the vortex center point position and core radius.

Comparing the results at plane $x/c = 1$, the UVLM data is relatively accurate in both vortex core position and size. While vortex cores typically project towards the inboard and downward direction [14], the results from UVLM appear to shift too rapidly when it goes downstream. The core radius also exhibits an accelerated growth rate. The discrepancy arises because the UVLM is a numerical model that utilizes discrete panel representation to approximate the wake vortex behavior. This reduces the computational complexity compared to higher-order models but can impact the prediction accuracy, especially for the highly dynamic wingtip vortices downstream. Based on the wingtip circulation, vortex center location and core radius derived from UVLM, the data at plane $x/c = 1$ demonstrates the most promising outcome amongst the planes, showing closely matched profile with reference data. Therefore, it will be utilized to populate the velocity components required for the LES MS inlet boundary conditions using the formulations (8) to (12). The results of LES MS domain with the inlet boundary specified by the $x/c = 1$ plane data from UVLM are shown in Figure 9.

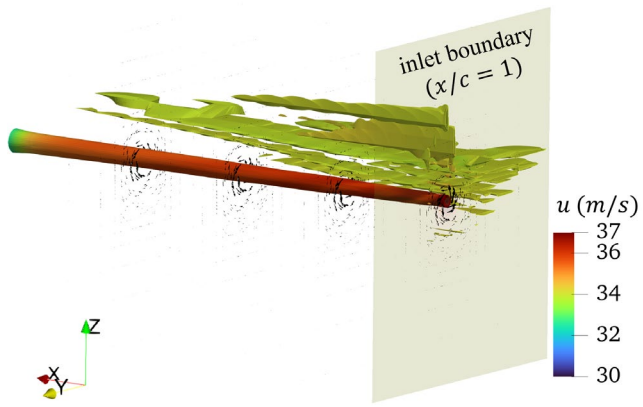

Figure 9: LES main simulation (MS) with the mean inflow conditions derived from UVLM, visualized with Q-criterion and colored by the velocity magnitude.

Since the mean flow field data prescribed with the UVLM aims to provide an efficient approach to initialize the wingtip vortex flow in a LES inlet condition, the mean vortical velocities remain constant throughout the simulation. Therefore, the wingtip vortices in the LES MS do not exhibit any turbulence-like structure, as shown in Figure 9. In comparison to Figure 4, the vortex core appears to maintain a relatively consistent core diameter downstream. To examine the vortex development with the inlet conditions initialized by UVLM, the flow field quantities across the vortex core in the cutting planes are extracted for assessment against the published data [18]. The comparisons on the tangential and axial velocities are illustrated in Figure 10 and Figure 11, respectively.

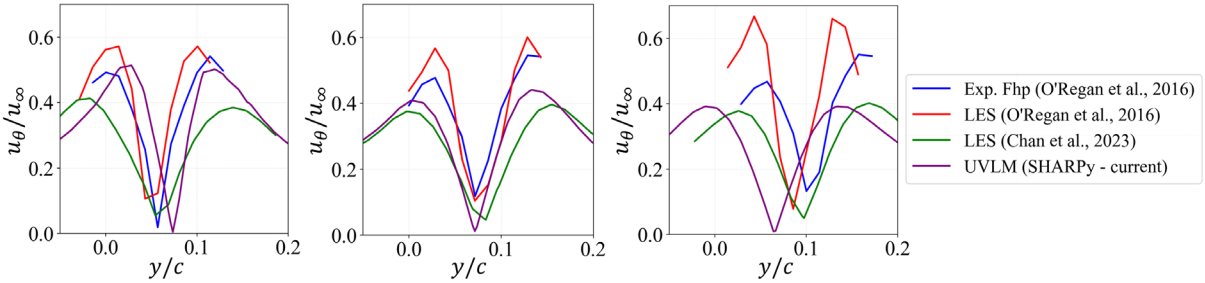

(a) $x/c = 1$ (b) $x/c = 2$ (c) $x/c = 3$

Figure 10: Validation on normalized tangential velocity magnitude u_θ/u_∞.

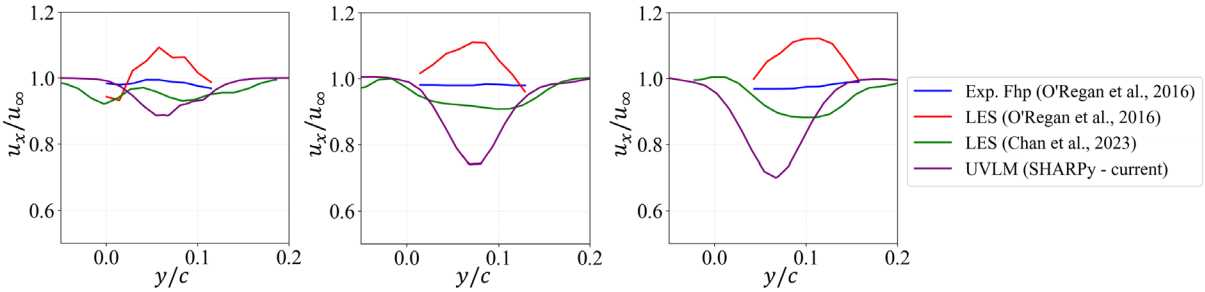

(a) $x/c = 1$ (b) $x/c = 2$ (c) $x/c = 3$

Figure 11: Validation on normalized tangential velocity magnitude u_x/u_∞.

At the inlet boundary ($x/c = 1$), the inlet condition by UVLM is showing the right vortex characteristic as per expected. The tangential velocity peaks and the trough are at similar locations, indicating the center position and radius of the vortex core. The magnitude is slightly higher than the LES data, likely due to the smaller core radius specified. The axial velocity also exhibits a deficit of approximately 15%, as defined by the equation (12).

As the flow develops downstream, it is noticed that while the tangential velocity maintains a satisfactory level of magnitude, the position of the vortex core remains stationary, with its center fixed at $0.07c$ inboard. Similarly, the trough position of the axial velocity deficit does not shift as predicted by the LES data. Moreover, the deficit profile diverges further from the LES charts, possibly due to the overly specified initial deficit value. The discrepancies in the core position are caused by the absence of time-varying velocity components at the inlet boundary. In LES, the fluctuation components play a crucial role in computing the kinetic energy and the Reynolds stress tensor. These parameters in turn affect the flow dynamics and turbulence characteristics within the domain, resulting in inaccuracies in vortex development. The fluctuations level of the inlet velocities is however correlated with both the spatial and temporal scale. Hence, in the following section, the authors are exploring the development of representative fluctuations at the inlet conditions from LES.

3.2 Synthesized Fluctuations from LES

Wingtip vortices feature a vortex core characterized by intense tangential velocity and a deficit in axial velocity. Hence, the three-dimensional velocity components and their respective fluctuation levels vary significantly across the inlet plane. To synthesize the mean-velocity inlet conditions generated from UVLM, it is necessary to derive the dedicated synthetic Fourier series equations for each directional component. Therefore, the UVLM case setup is replicated in LES to simulate the generation of wingtip vortices. The airfoil profile is NACA0012 instead of flat plat, and the flight condition corresponds to a chord-based Reynolds number of $Re_c = 3.25 \times 10^{-5}$.

The simulation focuses on capturing the time-series fluctuations incorporated with the vortex flow and utilizing them to reproduce the representative turbulence on the constant inlet conditions. Figure 12 illustrates the airflow over the NACA0012 wing with $\alpha = 10°$, the wake vortex is characterized by a tube-like vortex core structure along the streamwise direction. This core structure is accompanied by turbulence induced by flow separation from the wing geometry. It shows a more realistic flow field representation on the wingtip vortex as compared to Figure 9. The study will investigate the velocity fluctuations at the plane $x/c = 1$, which corresponds to the inlet plane as defined by UVLM.

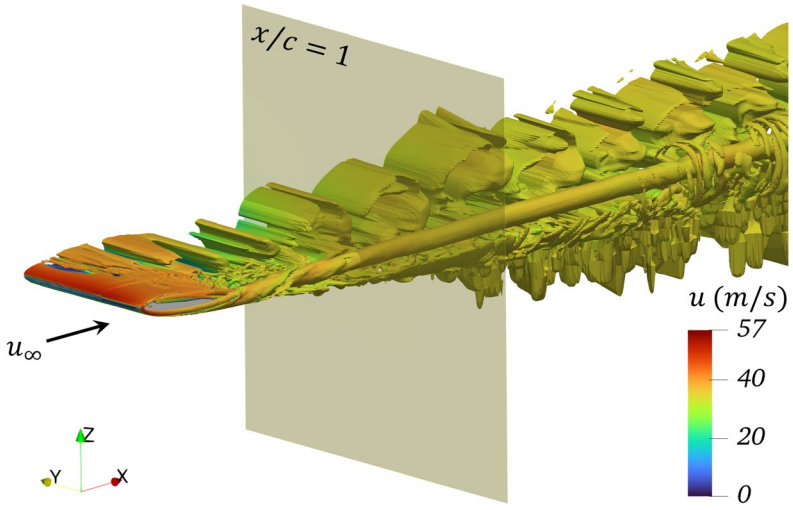

Figure 12: Wake vortex in LES IC domain visualized with Q-criterion, colored by velocity magnitude.

On the plane of $x/c = 1$, the point with the highest tangential velocity is chosen as the reference point for deriving the fluctuation profile. It is positioned at the circumference of the vortex core radius,

representing the most kinetic and energetic region within the plane. The three-dimensional time series velocity fluctuation is normalized by the mean velocity magnitude at the selected point and plotted in Figure 13, to provide a perspective on the relative fluctuations observed at the most dynamic points within the plane.

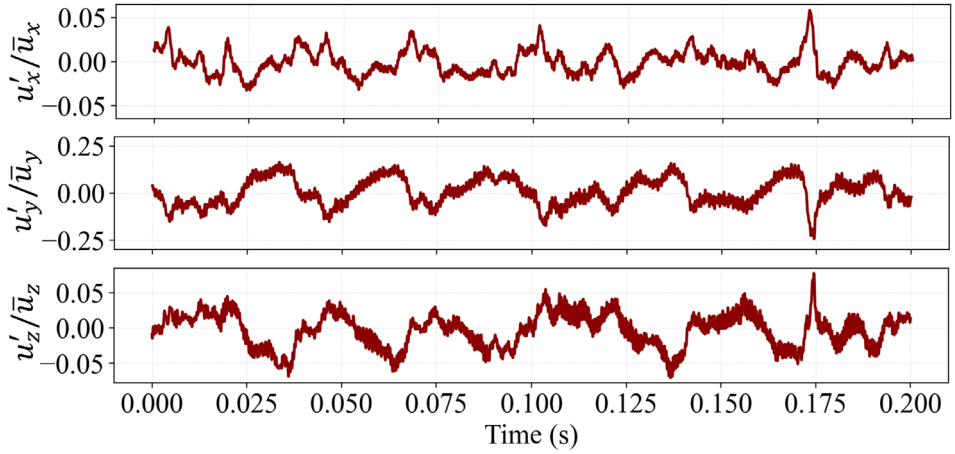

Figure 13: Time domain plot of the normalized velocity fluctuations, $u'/\bar{u}$ on the point with maximum tangential velocity, $u_{\theta,max}$ at plane $x/c = 1$ in LES IC.

Direct utilization of the time domain data in synthetic method is not feasible, the data must be transformed into frequency domain to enable the extraction of crucial parameters for the sinusoidal equations such as amplitude, frequency and phase lag. The frequency domain plot in Figure 14 reveals that the spectral peaks are prominently concentrated below 500Hz, consistent with the observations reported in other literature with moderate Reynolds number [67]. In addition, there are some minor amplitude peaks detected in the frequency spectrum between 1kHz and 3kHz.

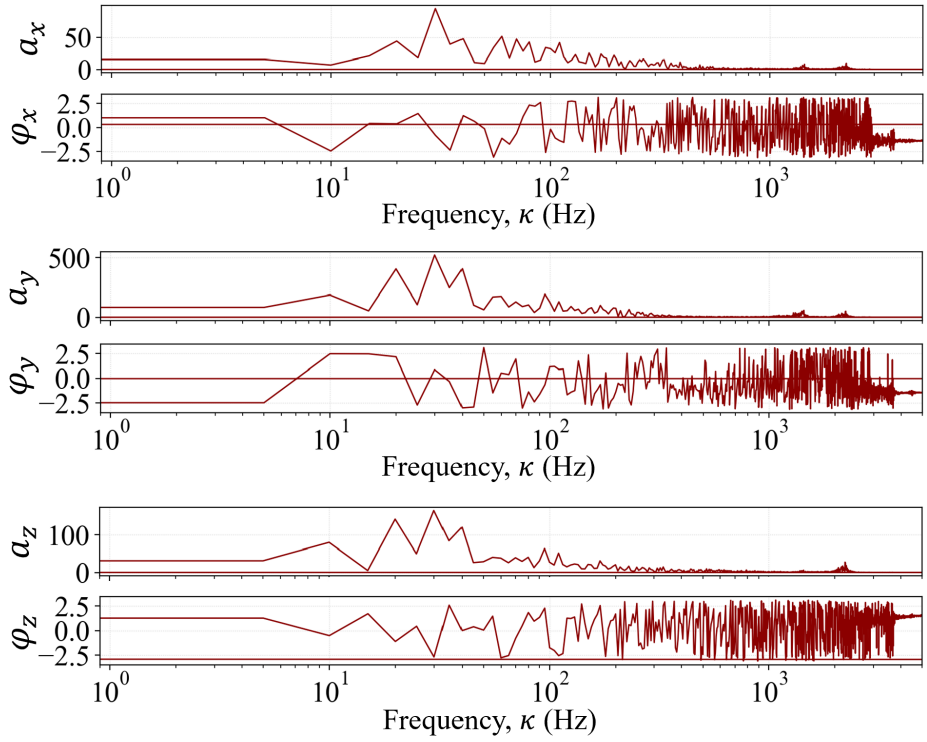

Figure 14: Frequency domain plot in amplitude, $a_{i,j,k}$ and phase, $\varphi_{i,j,k}$spectrum, corresponding to the time domain plot in Figure 13.

The wake roll-up from the wingtip is associated with the small-scale turbulence which are characterized by high frequency fluctuations [68]. For instance, at the plane near to the turbulent boundary layer ($x/c = 0$), the high frequency fluctuations are equally dominant as those lower frequencies. However, as the wake vortex evolves downstream, the intensities of high frequency fluctuations gradually diminish as shown in Figure 15. The velocity fluctuations of the wake vortex are transitioning towards lower frequency and higher amplitude as it progresses beyond the unsteady separation. This phenomenon explains the observation in Figure 14, where the flow dynamics are mainly driven by the lower frequency fluctuations, while the high frequency fluctuations manifest with minimal amplitudes due to the remnants of small eddies.

Figure 15: Velocity fluctuations contour in the LES IC domain, at planes x/c =0, 1, 2 and 3.

With the corresponding amplitude, frequency and phase lag, the time series fluctuations synthesized by the Fourier series equations are plotted in Figure 16 to validate against the fluctuation profile from LES IC. In the diagram, despite the synthetic profile only exhibiting subtle high frequency perturbations along the chart, the general synthetic fluctuations closely resemble the inlet condition profile.

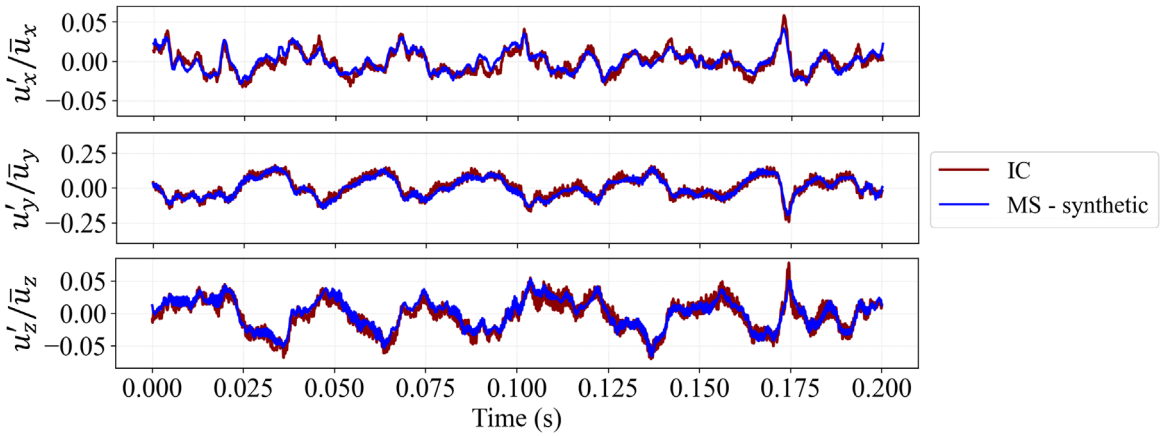

Figure 16: Validation of the time series synthesized fluctuations profile.

This validated synthetic formulation proves the feasibility of regenerating the velocity fluctuations on the LES inlet flow. Given that the validated fluctuations profiles are normalized by the mean velocity magnitude at the same spatial point, the synthesized method should be applicable to all grid points on the inlet, assuming the fluctuations magnitude is directly proportional to the respective directional mean velocity magnitude. This approach ensures that the fluctuations intensity applied across the vortex core are appropriately distributed according to their flow field activity. To validate this, the instantaneous velocity fluctuations across the vortex core are normalized by the mean velocity magnitude at each respective grid point in Figure 17. Fluctuations data across the vortex core are plotted along both the y-axis and z-axis to provide insights of how velocity fluctuations vary across the core in the two orthogonal directions. The objective is to achieve a nearly horizontal line with minimal deviation. This chart serves to indicate if the velocity fluctuations level is consistently conforming to a constant

percentage of their mean velocity magnitude across the vortex core.

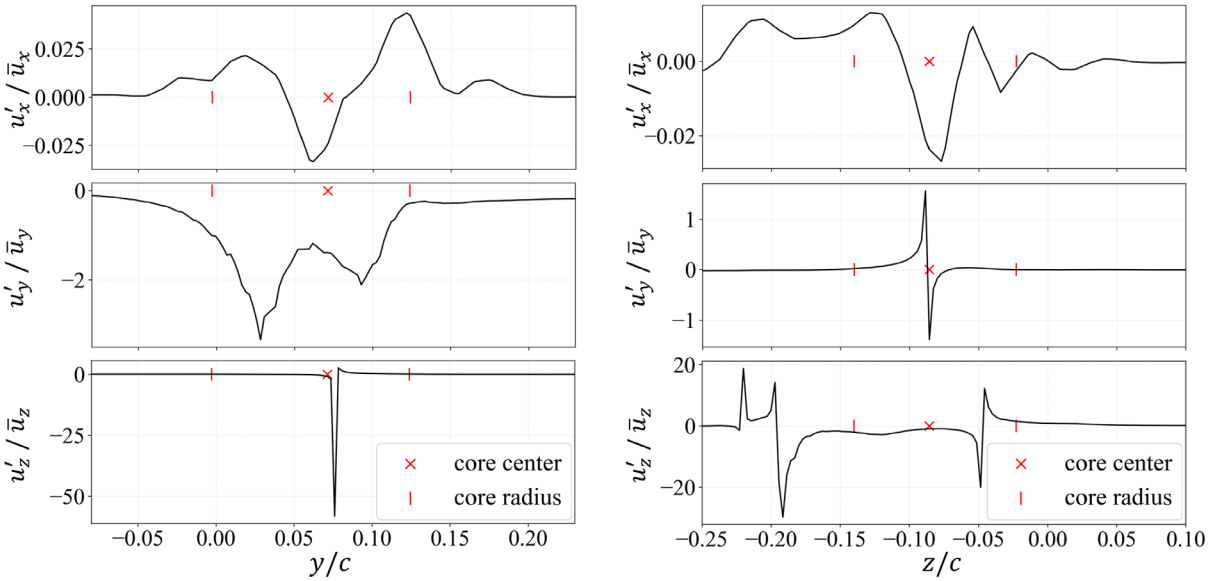

Figure 17: Normalized velocity fluctuations $u'/\bar{u}$ across vortex core in y-direction (left) and z-direction (right) at plane $x/c = 1$.

Figure 17 shows that the magnitude of fluctuations does not remain constant relative to the mean velocity magnitude, especially within the vortex core. Despite in the highly turbulent region, the normalized axial velocity fluctuation $u'_x / \bar{u}_x$ is maintained below ±3% along both axes. The axial velocity is largely driven by the freestream velocity, the fluctuations induced by the vortex shedding do not exert a significant influence over the dominant streamwise airflow. Along the measurement axis across vortex core, the velocity vector in parallel direction (u_y along y-axis, and u_z along z-axis) is near zero value due to the tangential velocity vector being perpendicular to the axis. Consequently, the normalized fluctuation errors tend to increase sharply near the core circumference. Despite the dominance of the crossflow velocity (u_z along y-axis, and u_y along z-axis), the vortex core is characterized by having near zero tangential velocity. This results in a spiking error at the core center region, affected area is less than 20% of the core diameter. The phenomenon is compounded by intense turbulent activities including flow perturbations and vortex core meandering, leading to significant spikes in both lateral and vertical fluctuations.

As a result, the synthesized Fourier series equation cannot be universally applied across all grid points on the inlet boundary. The potential strategy to address this limitation could involve incorporating conditional formulation in the synthesized fluctuation equations. An additional derivation on the fluctuation within vortex core is required to establish the conditional approach and to mitigate potential singularity errors.

4 Conclusion

The motivation for this research is driven by the CFD application of wake vortex surfing in extended longitudinal field. With the variety of formation configurations and positioning, evaluating the effects of vortex surfing on the trailing aircraft in each permutation will require extensive simulation efforts and substantial computational resources. To streamline this process, an efficient UVLM is employed to predetermine the wingtip vortex downstream. This vortex serves as the inlet conditions for the main LES simulation, effectively reducing the simulation domain size to begin just before the trailing

aircraft's position. This method also enables repeated assessments of aerodynamic performance across different aircraft types and positions.

The authors have successfully demonstrated the effective mapping of vortical flow from a UVLM model to the LES inlet boundary condition. Despite limitations of the UVLM model such as accelerated vortex core development, accurate representation of the vortex at the inlet of LES MS domain can be achieved through careful selection of the inflow. Future research may explore the correlation between the vortex growth rate in UVLM and actual cases. This will enable the identification of specific planes within UVLM that can be mapped onto the LES inlet to represent a more downstream plane.

Using the fluctuations characteristics extracted from a separated LES simulation, the authors formulated the Fourier series sinusoidal expression to synthesize the temporal velocity data. However, due to the unique flow dynamics within the vortex core, the normalized fluctuations technique that effectively regenerating the fluctuations on the mean velocity profile for most of the grid points is not applicable to certain areas or specific directional components. This highlights the challenges in specifying the accurate vortex velocity fluctuation on the inlet boundary condition. Future research will further derive the fluctuations within the core and focus on developing potential solutions, such as conditional mapping or introducing additional terms to improve the model.

In conclusion, this paper presented an efficient inlet mapping method tailored for the vortices in freestream airflow applications. This research differs from existing research which predominantly focuses on boundary layer turbulence in internal flows. The turbulence characteristics of vortex core are correlated in all directions and subject to specific growth and dissipation rates, highlighting the contribution of this research in advancing CFD techniques for studying wake vortex interactions and their effects on trailing aircraft performance.

References

[1] W. B. Blake, S. R. Bieniawski and T. C. Flanzer, "Surfing aircraft vortices for energy," *The Journal of Defense Modeling and Simulation: Applications, Methodology, Technology,* vol. 12, no. 1, pp. 31-39, 2013.

[2] Y. Zhao, H. Wu, Q. Zhang and Q. Cheng, "Overview of surfing aircraft vortices for energy," *Journal of Physics: Conference Series (The 11th Asia Conference on Mechanical and Aerospace Engineering ACMAE),* vol. 1786, no. 1, pp. 12-26, 2021.

[3] P. B. S. Lissaman and C. A. Shollenberger, "Formation Flight of Birds," *Journal of Science,* vol. 168, no. 3934, pp. 1003-1005, 1970.

[4] H. Weimerskirch, J. Martin, Y. Clerquin, P. Alexandre and S. Jiraskova, "Energy saving in flight formation," *Nature,* vol. 413, no. 6857, pp. 697-698, 2001.

[5] D. Fleischmann and M. M. Lone, "Analysis of wake surfing benefits using a fast unsteady vortex lattice method," *AIAA Scitech 2019 Forum,* 2019.

[6] D. Hummel, "Formation flight as an energy-saving mechanism," *Israel Journal of Zoology,* vol. 41, no. 3, pp. 261-278, 1995.

[7] L. R. Jenkinson, R. E. Caves and D. P. Rhodes, "Automatic formation flight - A preliminary investigation into the application to civil operations," *Aircraft Engineering, Technology, and Operations Congress,* 1995.

[8] E. Wagner, "An Analytical Study of T-38 Drag Reduction in Tight Formation Flight," Master Thesis, Department of The Air Force, Air University, Air Force Institute of Technology, Wright-Patterson Air Force Base, Ohio, 2002.

[9] E. Wagner, D. Jacques, W. Blake and M. Pachter, "Flight Test Results of Close Formation Flight for Fuel Savings," *AIAA Atmospheric Flight Mechanics Conference and Exhibit,* 2002.

[10] J. Pahle, D. Berger, M. Venti, C. Duggan, J. Faber and K. Cardinal, "An Initial Flight Investigation of Formation Flight for Drag Reduction on the C-17 Aircraft," *AIAA Atmospheric Flight Mechanics Conference,* 2012.

[11] O. B. Escarre, T. d. U. Cantavenera, G. Martin and M. A. Piera, "Modeling flight pairing strategies for formation flights in continental airspace," in *35th European Modeling & Simulation Symposium*, Barcelona, Spain, 2023.

[12] J. Adams, C. Frot and G. Ta, "The Vortex Position Estimator used for the Airbus fello'fly Trasnatlantic Crossing," in *Conference on Guidance, Navigation and Control*, Berlin, Germany, 2022.

[13] C. Breitsamter, "Wake vortex characteristics of transport aircraft," *Progress in Aerospace Sciences,* vol. 47, no. 2, pp. 89-134, 2011.

[14] J. C. Chan, H. Hesse and P. C. Wang, "Wingtip Vortices Characterization with Perspective Upright Correction," in *AIAA AVIATION 2023 Forum*, San Diego and Online, 2023.

[15] D. Singh, A. F. Antoniadis, P. Tsoutsanis, H.-S. Shin, A. Tsourdos, S. Mathekga and K. W. Jenkins, "A Multi-Fidelity Approach for Aerodynamic," *Aerospace,* vol. 5, no. 2, p. 66, 2018.

[16] D. Zhang, Y. Chen, X. Dong, Z. Liu and Y. Zhou, "Numerical Aerodynamic Characteristics Analysis of the Close Formation Flight," *Mathematical Problems in Engineering,* pp. 1-13, 2018.

[17] R. H. Bush, T. Chyczewsky, K. Duraisamy, B. Eisfeld, C. L. Rumsey and B. R. Smith, "Recommendations for Future Efforts in RANS Modeling and Simulation," *AIAA SciTech Forum,* 2019.

[18] J. C. Chan, P. C. Wang and H. Hesse, "Aerodynamic Interactions in Formation Flight for Wake Vortex Surfing," in *AIAA AVIATION 2023 Forum*, San Diego and Online, 2023.

[19] C. H. Moeng and P. P. Sullivan, Large-Eddy Simulation, National Center for Atmospheric Research, Boulder, CO, USA, 2015.

[20] B. Chaouat, "The State of Art of Hybrid RANS/LES Modeling for the Simulation of Turbulent Flows," *Springer Science+Business Media,* pp. 279-327, 2017.

[21] P. Moin and K. Mahesh, "DIRECT NUMERICAL SIMULATION: A Tool in Turbulence Research," *Annu. Rev. Fluid Mech.,* vol. 30, pp. 539-578, 1998.

[22] D. Vechtel, D. Fischenberg and J. Schwithal, "Flight dynamics simulation of formation flight for energy saving using LES-generated wake flow fields," *CEAS Aeronautical Journal,* vol. 9, no. 4, pp. 735-746, 2018.

[23] P. C. Wang and J. J. McGuirk, "Large Eddy Simulation of HIgh Speed Nozzle Flows - Assessment & Validation of Synthetic Turbulence Inlet Conditions," in *20th AIAA Computational Fluid Dynamics Conference*, Honolulu, Hawaii, 2011.

[24] J.-L. Aider, A. Danet and M. Lesieur, "Large eddy simulation applied to study the influence of upstream conditions on the time-dependant and averaged characteristics of a backward-facing step flow," *Journal of Turbulence,* vol. 8, no. 51, 2007.

[25] M. H. Baba-Ahmadi and G. Tabor, "Inlet conditions for LES using mapping and feedback control," *Computers & Fluids,* vol. 38, pp. 1299-1311, 2009.

[26] G. R. Tabor and M. H. Baba-Ahmadi, "Inlet conditions for large eddy simulation: A review," *Computers & Fluids,* vol. 39, pp. 553-567, 2010.

[27] P. C. Wang and J. J. McGuirk, "Large Eddy Simulation of supersonic jet plumes from rectangular con-di nozzles," *International Journal of Heat and Fluid Flow,* vol. 43, pp. 62-73, 2013.

[28] P. C. Wang and J. J. McGuirk, "Validation of a large eddy simulation methodology for accelerated nozzle flows," *The Aeronautical Journal,* vol. 124, no. 1277, pp. 1070-1098, 2020.

[29] A. Montorfano, F. Piscaglia and G. Ferrari, "Inlet boundary conditions for incompressible LES: A comparative study.," *Mathemarical and Computer Modelling,* vol. 57, no. 7-8, pp. 1640-1647, 2013.

[30] E. D. Villers, "The Potential of Large Eddy Simulation for the Modelling of Wall Bounded Flows," Department of Mechanical Engineering Imperial College London, London, 2006.

[31] N. S. Dhamankar, G. A. Blaisdell and A. S. Lyrintzis, "Overview of Turbulent Inflow Boundary Conditions for Large-Eddy Simulations," *AIAA Journal,* vol. 56, no. 4, 2017.

[32] C. D. Pierce and P. Moin, "Method for Generating Equilibrium Swirling Inflow Conditions," *AIAA Journal,* vol. 36, no. 7, pp. 1325-1327, 1998.

[33] X. Jiang , G. A. Siamas and L. C. Wrobel, "Analytical Equilibrium Swirling Inflow Conditions for Computational Fluid Dynamics," *AIAA Journal,* vol. 46, no. 4, pp. 1015-1018, 2008.

[34] K. Kondo, S. Murakami and A. Mochida, "Generation of velocity fluctuations for inflow boundary condition of LES," *Journal of WInd Engineering and Industrial Aerodynamics,* vol. 67&68, pp. 51-64, 1997.

[35] P. Sagaut, in *Large Eddy Simulation for Incompressible Flows: An Introduction*, Berlin, Germany, Springer, 2013.

[36] J. Murua, R. Palacios and J. M. R. Graham, "Applications of the unsteady vortex-lattice method in aircraft aeroelasticity and flight dynamics," *Progress in Aerospace Sciences,* vol. 55, pp. 46-72, 2012.

[37] J. U. Schluter, H. Pitsch and P. Moin, "Large-Eddy Simulation Inflow Conditions for Coupling with Reynolds-Averaged Flow Solvers," *AIAA Journal,* vol. 42, no. 3, 2004.

[38] S. Benhamadouche, N. Jarrin, Y. Addad and D. Laurence , "Synthetic turbulent inflow conditinos based on a vortex method for large-eddy simulation," *Progress in Computational Fluid Dynamics,* vol. 6, no. 1/2/3, pp. 50-57, 2006.

[39] K.-S. Yang and J. H. Ferziger, "Large-Eddy Simulation of Turbulent Obstacle Flow Using a Dynamic Subgrid-Scale Model," *AIAA Journal,* vol. 31, no. 8, pp. 1406-1413, 1993.

[40] R. G. Deissler, "Turbulent Fluid Motion V-Fourier Analysis, the Spectral Form of the Continuum Equations, and Homogeneous Turbulence," NASA Lewis Research Center, Cleveland, Ohio, 1996.

[41] M. Kaushuk, Theoretical and Experimental Aerodynamics, Kharagpur, West Bengal, India: Springer, 2019.

[42] J. Katz and A. Plotkin, Low-speed aerodynamics, Cambridge: Cambridge University Press, 2001.

[43] R. Palacios, "SHARPy: Simulation of High-Aspect-Ratio aircraft and wind turbines in Python," Imperial College London, 12 September 2023. [Online]. Available: https://www.imperial.ac.uk/aeroelastics/sharpy/. [Accessed 12 February 2024].

[44] A. del Carre, A. Muñoz-Simón, N. Goizuera and R. Palacios, "SHARPy: A dynamic aeroelastic simulation toolbox for," *Journal of Open Source Software,* vol. 4, no. 44, p. 1885, 2019.

[45] H. Hesse and R. Palacios, "Dynamic Load Alleviation in Wake Vortex Encounters," *Journal of Guidance, Control, and Dynamics,* vol. 39, no. 4, pp. 801-813, 2016.

[46] S. Düssler and R. Palacios, "Enhanced Unsteady Vortex Lattice Aerodynamics for Nonlinear Flexible Aircraft Dynamic Simulation," *AIAA Journal,* vol. 62, no. 3, pp. 1179-1194, 2024.

[47] J. Murua, R. Palacios and J. M. R. Graham, "Assessment of Wake-Tail Interference Effects on the Dynamics of Flexible Aircraft," *AIAA Journal,* vol. 50, no. 7, pp. 1575-1585, 2012.

[48] S. Deng, C. Jiang, Y. Wang and H. Wang, "Acceleration of unsteady vortex lattice method via dipole panel fast multipole method," *Chinese Journal of Aeronautics,* vol. 34, no. 2, pp. 265-278, 2021.

[49] F. Holzapfel, T. Gerz, M. Frech and A. Dornbrack, "Wake Vortices in Convective Boundary Layer and Their Influence on Following Aircraft," *Journal of Aircraft,* vol. 37, no. 6, pp. 1001-1007, 2000.

[50] N. N. Ahmad, F. H. Proctor, F. M. L. Duparcmeur and D. Jacob, "Review of Idealized Aircraft Wake Vortex Models," in *AIAA SciTech 52nd Aerospace Sciences Meeting*, National Harbour, Maryland, 2014.

[51] S. Gudmundsson, "Chapter 9 - The Anatomy of the Wing," in *General aviation aircraft design: Applied Methods and Procedures*, Butterworth-Heinemann, 2014, pp. 299-399.

[52] M. Xu, H. Cheng, B. Ji and X. Peng, "Prediction method of tip vortex circulation based on hydrofoil load," *Ocean Engineering,* vol. 288, p. 116176, 2023.

[53] D. H. Thompson, "Experimental study of axial flow in wing tip vortices," *Journal of Aircraft,* vol. 12, no. 11, pp. 910-911, 1975.

[54] S. Ragab and M. Sreedhar, "Numerical simulation of vortices with axial velocity deficits," *Physics of Fluids,* no. 7, pp. 549-558, 1995.

[55] W. J. Devenport, M. C. Rife, S. I. Liapia and G. J. Follin, "The structure and development of a wing-tip vortex," *Journal of Fluid Mechanics,* vol. 312, pp. 67-106, 1996.

[56] The OpenFOAM Foundation, "OpenFOAM," n.d.. [Online]. Available: https://openfoam.org/. [Accessed 22 Nov 2023].

[57] K. J. B. Tan, P. C. Wang and S. Srigrarom, "Low-Speed Post-Stall Wing Wake Impingement on Horizontal Stabilizer of the Common Research Model," in *Aviation Technology, Integration, adn Operations Conference*, Atlanta. Georgia, 2018.

[58] K. J. B. Tan, H. Hesse and P. C. Wang, "Wing-Tail Interaction Under Forced Harmonic Pitch," in *AIAA Aviation Forum*, Virtual Event, 2021.

[59] J. Smagorinsky, "General circulation experiments with the primitive equations," *Monthly Weather Review,* vol. 91, no. 3, pp. 99-164, 1963.

[60] D. Carati, G. S. Winckelmans and H. Jeanmart, "On the modelling of the subgrid-scale and filtered-scale stress tensors in large-eddy simulation," *Journal of Fluid Mechanics,* vol. 441, pp. 119-138, 2001.

[61] K. J. B. Tan, H. Hesse and P. C. Wang, "Numerical Capture and Validation of a Massively Separated Bluff-Body Wake," in *AIAA Aviation Forum*, Virtual Event, 2020.

[62] T. A. Smith and Y. Ventikos, "Wing-tip vortex dynamics at moderate Reynolds numbers," *Physics of Fluids,* vol. 33, 2021.

[63] F. Mathey, D. Cokljat, J. P. Bertoglio and E. Sergent, "Assessment of the vortex method for Large Eddy Simulation inlet conditons," *Progress in Computational Fluid Dynamics,* vol. 6, no. 1/2/3, pp. 58-67, 2006.

[64] J. C. Chan, H. Hesse and P. C. Wang, "Inlet Mapping of Wingtip Vortices in LES for Wake Vortex Surfing," in *AIAA Aviation Forum*, Las Vegas, Nevada, 2024.

[65] K. Kondo, S. Murakami and A. Mochida, "Generation of velocity fluctuations for inflow boundary condition of LES," *Journal of Wind Engineering and Industrial Aerodynamics,* vol. 67&68, pp. 51-64, 1997.

[66] M. S. O'Regan, P. C. Griffin and T. M. Young, "A vorticity confinement model applied to URANS and LES simulations of a wing-tip vortex in the near-field," *International Journal of Heat and Fluid Flow,* vol. 61, pp. 355-365, 2016.

[67] T. A. Smith and Y. Ventikos, "Wing-tip vortex dynamics at moderate Reynolds numbers," *Physics of Fluids,* vol. 33, no. 3, 2021.

[68] M. Wang and P. Moin, "Computation of Trailing-Edge Flow and Noise Using Large-Eddy Simulation," *AIAA Journal,* vol. 38, no. 12, pp. 2201-2209, 2000.

[69] M. Parenteau, E. Laurendeau, F. Plante and M. Costes, "Unsteady Coupling Algorithm for Lifting-Line Methods," in *55th AIAA Aerospace Sciences Meeting*, Grapevine, Texas, 2017.